Applied Thermal Engineering 129 (2018) 884–892

Contents lists available at ScienceDirect

Applied Thermal Engineering

journal homepage: www.elsevier.com/locate/apthermeng

Research Paper

# Energy harvesting via fluidic agitation of a magnet within an oscillating heat pipe

J. Gabriel Monroe [a], Omar T. Ibrahim [b], Scott M. Thompson [c,*], Nima Shamsaei [c]

[a] Engineer Research and Development Center (ERDC), US Army Corps of Engineers, Vicksburg, MS 39180, USA
[b] Department of Mechanical Engineering, Mississippi State University, Starkville, MS 39762, USA
[c] Department of Mechanical Engineering, Auburn University, Auburn, AL 36849, USA

## HIGHLIGHTS

- Oscillating heat pipes (OHPs) can be used for thermal energy conversion.
- Fluid motion within an OHP can agitate a suspended magnet for induction.
- Thermal performance of OHP harvester increases at cost of power generation.
- Suspending larger magnets within OHP tube can increase power generation.
- OHP harvester is a portable means for electric power generation.

## ARTICLE INFO

*Article history:*
Received 10 May 2017
Revised 7 October 2017
Accepted 12 October 2017
Available online 13 October 2017

*Keywords:*
Pulsating heat pipe
Energy harvesting
Energy conversion
Electric generator
Thermoelectric
Electromagnetic

## ABSTRACT

An 'oscillating magnet' energy harvesting module was developed and integrated into a 4-turn, tubular oscillating heat pipe (OHP) filled with water. The harvesting module consisted of a 1000-turn solenoid wrapped around a polycarbonate tube and two transverse posts, which were placed through the tube above and below the solenoid. Electromagnetic induction was accomplished via the thermally-driven, fluidic agitation of a suspended neodymium magnet placed between the transverse posts. The thermal performance and energy harvesting ability of this 'oscillating-magnet OHP' (OMHP) was experimentally investigated over a range of heat inputs with either 1.59 mm or 3.17 mm diameter neodymium magnets. Results demonstrate that the OMHP heat transfer performance decreased as the magnet diameter approached that of the OHP tube due to increased local pressure drops across the magnet, which disrupted advection between the evaporator and condenser. At 400 W of heat input, the OMHP equipped with a smaller oscillating magnet (*i.e.* 1.59 mm diameter) produced a maximum peak electrical power of 21.9 μW and provided an effective thermal conductivity of ~7000 W/m K. In contrast, the OMHP equipped with a larger oscillating magnet (*i.e.* 3.17 mm diameter) produced a maximum peak electrical power of 428 μW and an effective thermal conductivity of ~2600 W/m K at 200 W of heat input. Since the confined magnet motion is coupled with the heat transfer and internal fluid motion of the OHP, the design of the OMHP is driven by the importance of energy harvesting relative to thermal performance. This technology is unique in that it can be used for thermal management and in situ electric power production.



## 1. Introduction

The oscillating heat pipe (OHP) is a two-phase heat transfer device comprised of an evacuated serpentine capillary tube/channel structure, partially filled with a working fluid (*e.g.* water, refrigerant, dielectric fluids, etc.), that spans between a heat source (*i.e.* evaporator) and a heat sink (*i.e.* condenser) [1,2]. Unlike other types of heat pipes, a wicking structure is not required for effectively pumping liquid from the condenser to the evaporator. Instead, the heated (and cooled) portions of the serpentine-arranged capillary lead to evaporation (and condensation) of various-sized liquid (and vapor) slugs, thus leading to a highly-unstable, non-uniform vapor pressure field that supports non-equilibrium thermomechanical conditions. This 'imbalanced' fluid mixture and pressure distribution results in the pulsation and circulation of the entrained fluid; typically over a spectrum of

* Corresponding author at: Department of Mechanical Engineering, Auburn University, 1418 Wiggins Hall, 354 War Eagle Way, Auburn, AL 36849, USA.
*E-mail address:* smthompson@auburn.edu (S.M. Thompson).

https://doi.org/10.1016/j.applthermaleng.2017.10.076
1359-4311/

**Nomenclature**

| | |
|---|---|
| $d$ | diameter, mm |
| $g$ | acceleration due to gravity, m/s$^2$ |
| $k_{eff}$ | effective thermal conductivity, W/m K |
| $N$ | number of coils in a solenoid |
| $p$ | pressure, kPa |
| $P$ | power, W |
| $Q$ | heat transfer, W |
| $r$ | radius, mm |
| $R$ | resistance, Ω |
| $t$ | time, s |
| $t\#$ | OMHP tube number |
| $T$ | temperature, °C |
| $V$ | voltage, mV |
| $VAC$ | alternating current voltage, mV |
| $VOC$ | open circuit voltage, mV |
| $\Delta y$ | longitudinal distance between thermocouples in adiabatic region |
| $\Delta T$ | temperature difference, $\Delta^o$C |

*Greek symbols*

| | |
|---|---|
| $\varepsilon$ | electromotive force (EMF), mV |
| $\Phi$ | magnetic flux, Wb |
| $\rho$ | density, kg/m$^3$ |
| $\sigma$ | surface tension, N/m |

*Subscripts*

| | |
|---|---|
| avg | average |
| i | internal |
| l | liquid |
| o | outer |
| pp | peak-to-peak (voltage) |
| r | resistor |
| s | solenoid |
| v | vapor |

frequencies less than 10 Hz [3–6]. A minimum temperature difference (or heat flux) is required to ensure sufficient latent heat transfer for initiating and sustaining fluid motion within the OHP [7,8]. This latent heat transfer accounts for ~10–20% of overall OHP thermal transport [9], while fluid motion between the evaporator and condenser allows for sensible heat transfer via forced convection - a dominant energy transport mechanism within the OHP. The cumulative effect of all transport mechanisms within the OHP is an effective thermal conductivity on the order of $10^3$ or $10^4$ W/m K [10], broadening its appeal for use in many thermal management applications. In an operational sense, the upper limit of an OHP's usefulness is evaporator 'dry-out', which occurs when a sufficiently large heat flux prevents liquid from returning to the evaporator [11]. OHPs with lower fluid filling ratios (*i.e.* the ratio of liquid volume to the total OHP channel volume) are typically more susceptible to dry out at lower heat fluxes due to pressure balancing in the evaporator.

To date, the majority of OHP research has focused on characterizing and modeling [4,12,13] its thermal performance and its relation to various free design/conditional variables (*e.g.* channel geometry, fluid fill ratio, fluid properties, orientation, heat source, etc.). Distinct applications of OHPs have also been investigated, including their use for waste heat recovery in HVAC [14] and energy storage systems [15], as well as thermal management of cryopreservation systems [16] and electromagnetic launchers [17]. The use of OHPs for energy harvesting has also been inspected. Zabek et al. [18] demonstrated OHP thermal-to-electric conversion using pyroelectric elements atop the surface of a copper FP-OHP. The vapor bubbles and liquid plugs oscillating inside the FP-OHP caused surface temperature variations of ~5 K at frequencies of ~0.45 Hz. The transient temperature field resulted in the pyroelectric array producing a maximum open circuit voltage of 0.8 VAC. Recently, Monroe et al. [19] demonstrated the ability of a 'ferrofluid OHP' (FF-OHP) to generate electricity through thermal-to-electrical energy conversion. The FF-OHP was partially filled with water/$Fe_3O_4$ ferrofluid and a 1000-turn solenoid wrapped around a section of the OHP tube. In order to align the magnetic dipoles of the ferro-nanoparticles, the FF-OHP was placed between two 16.4 cm$^3$ cube neodymium magnets for creating a static 'bias' magnetic field, which temporarily magnetized the ferrofluid. During operation, the unstable FF-OHP pressure field forced suspended/magnetized ferro-nanoparticles to pass through the solenoid resulting in 'ferrofluidic induction' and voltage generation on-the-order of 1 mV. Others have also demonstrated ferrofluidic induction using actively-pumped/shaken ferrofluids in adiabatic systems of larger dimensions (> capillary scale) [20–22].

Similar to ferrofluidic induction is the operating principle of a linear electric generator (LEG). In both cases, Faraday's law is exploited for generating an electromotive force across a solenoid in-proximity to an accelerating magnetic medium. In a classical LEG, an electrical/alternating current is produced via the relative, collinear motion between a magnetized medium and a static, adjacent (or co-axial) solenoid. Many features of the LEG (*e.g.* stroke length, magnet size, etc.) can be designed for various size/power requirements in order to achieve small-to-very-large power outputs [23–27]. The propulsion of the magnet may be cyclically driven via forced mechanical work or randomly driven via harvested mechanical work, *e.g.* from roadways [28], ocean waves [26], human motion [24] and vibration from combustion cycles [29].

The present study introduces a new means to use an OHP for accomplishing thermal-to-electrical energy conversion. In particular, a method for driving a LEG via the thermally-driven, mechanical agitation of a permanent magnet suspended within an OHP is described. The thermal performance of this 'oscillating-magnet' OHP (OMHP) and its coupling to electric power generation are discussed and supported with experimental results.

## 2. Experimental description

### 2.1. Electromagnetic considerations

Electromagnetic induction may be stated mathematically using Faraday's law, which states that a time varying magnetic field induces an electromotive force, $\varepsilon$, in an electrical conductor. Eq. (1) describes this relationship for an $N$-turn solenoid electrical conductor.

$$\varepsilon = -N\frac{\partial \vec{B}}{\partial t} \tag{1}$$

Inspection of Eq. (1) gives direction for the design and testing of the OMHP harvesting module and suggests larger $\varepsilon$ is achievable by increasing $N$ and/or the magnitude of $\partial \boldsymbol{B}/\partial t$. With regards to a magnet in motion, $\partial \boldsymbol{B}/\partial t$ increases with magnet size (*i.e.* maximum field strength) and speed (*i.e.* rate of change upon approach and departure).

An OMHP is a unique embodiment of a LEG in that oscillations are temperature-driven and power production is accompanied by superior heat transfer ability. However, the introduction of the harvesting mechanism will have some effect on OHP baseline performance. Consideration of Eq. (1) and the adjoining, fundamental fluid dynamics can provide insight into possible OMHP behavior. For example, a smaller induction magnet (relative to OMHP tube size) has less inertia for the fluid flow to overcome, but a smaller face area reduces drag, which could allow the fluid to flow around the magnet without moving it. Rotation of smaller magnets is another possible concern for energy harvesting; however, such rotation can perhaps increase local heat transfer. Conversely, larger magnets may have higher induction potential due to stronger magnetic fields being generated, but the restricted flow around the magnet would have a larger impact on the thermal performance of the OMHP. Therefore, to explore the impact of energy harvesting on OMHP thermal performance, two induction magnets of the same length but differing diameters were employed in separate experiments, *i.e.* either a ∅1.59 mm (*i.e.* $OMHP_{1.59}$) or a ∅3.17 mm (*i.e.* $OMHP_{3.17}$), 6.35 mm long NdFeB-N52 magnet (each covering ~22% or ~87% of the harvesting tube cross-sectional area, respectively). The magnetic field of each magnet was simulated using Finite Element Method Magnetics (FEMM) v. 4.2 and a schematic of these simulated fields are shown in Fig. 1. The field simulations were verified based on measurements obtained using a gaussmeter (AlphaLabs, GM1-ST).

### 2.2. OMHP test setup

A 4-turn tubular OHP was fabricated from copper tubing (C12200 alloy) with ($d_i$, $d_o$) = (∅3.25, ∅4.8) mm. HPLC-grade water was selected as the working fluid due to its availability and well-documented behavior within the OHP. For standard terrestrial gravitational conditions (*i.e.* 1*g*), the capillary action of water (or any working fluid) is guaranteed within a conduit for Bond numbers ($\Delta\rho \cdot g \cdot d^2/\sigma$) ≤ 2 [30]. Hence, the maximum internal diameter of the OHP tubing was ensured to satisfy Eq. (2).

$$d_{max} \cong 2\sqrt{\frac{\sigma}{g \cdot (\rho_l - \rho_v)}} \cong 5 \text{ mm} \quad (2)$$

The OMHP was created by adding a LEG-based harvesting module to the adiabatic section of the OHP. The harvesting module was built around a 4.5 cm section of transparent, temperature-resistant polycarbonate tubing with ($d_i$, $d_o$) = (∅3.4, ∅9.5) mm ± 0.1 mm. A 1000-turn (±5 turns), 1.0 cm long solenoid was created by wrapping 0.125 mm diameter copper wire around the axial center of the polycarbonate tubing. An induction magnet was then placed inside the polycarbonate tube. To complete the harvester module, two ∅1.59 transverse copper posts were placed through the polycarbonate tubing – 1.9 cm above and below the solenoid center. The transverse posts prevented the fluid from carrying the magnet out of the harvesting module, but still allowed the magnet to repeatedly pass through the solenoid as it was buffeted by the oscillating fluid. The harvesting module was then installed in-line with a tubular section in the adiabatic section of the OMHP. Both the polycarbonate/copper tubing and polycarbonate/copper post interfaces were sealed with a two-part epoxy adhesive (J-B KWIK) to maintain hermeticity. The dimensions of the OMHP and the harvesting module are provided in Fig. 2. As shown in Fig. 2, nine type-T thermocouples (TCs) were affixed to the outside wall of the OMHP to quantify its thermal performance. Before each test, the OMHP was evacuated to less than 100 Pa using a centrifugal vacuum pump (Fisher Scientific® M8C) before being charged with HPLC-grade water to a 75% fill ratio (±2%). Once charged, the OMHP charging tube was pneumatically crimped to create a hermetic seal. The overall design of the OMHP matched that of the T-OHP used in [6].

Two aluminum water blocks were used for routing 15 °C (±0.5 °C) water from a recirculating bath (PolyScience AD15R-30-A11B) around the OMHP condenser for heat rejection. Two Ø = 10.2 cm, 300 W cartridge heaters were placed inside aluminum heating blocks for heating the OMHP. Cartridge heaters were connected to a powered, variable autotransformer (Staco Energy) for controlling the heat input. Because the cartridge heaters were placed across the width of the OMHP, each OMHP tube was subject to approximately the same heat flux. A digital multimeter (DMM) was used to measure the voltage output of the variable autotransformer. Power calculations were based on the parallel resistance of the cartridge heaters and the measured voltage output of the variable autotransformer (*i.e.* $P = V^2/R$). Grooves ($r \cong 2.4$ mm) matching

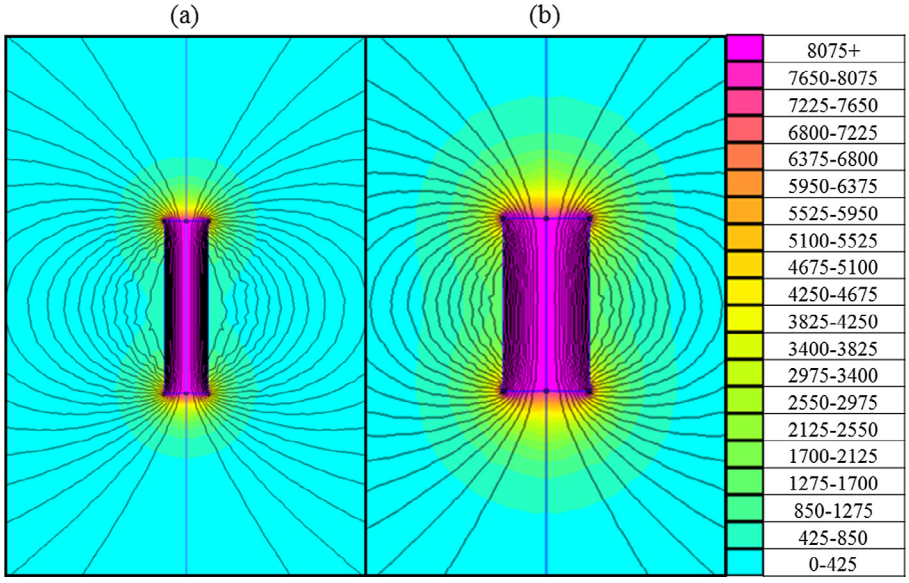


**Fig. 1.** Magnetic field lines and magnitude (colors corresponding to values listed on right in units gauss) of (a) ∅1.59 mm and (b) ∅3.17 mm LEG induction magnets (to scale).

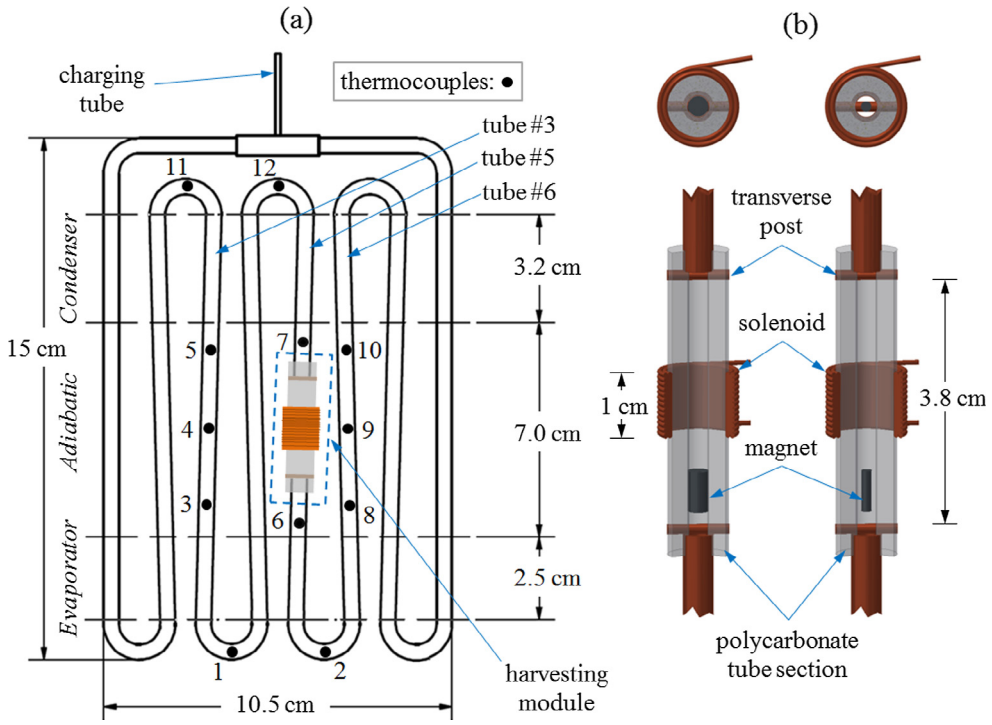


**Fig. 2.** Dimensions of (a) investigated OMHP with TC, evaporator, adiabatic, condenser, and harvesting module locations (not to scale) and (b) cut-away views with dimensions of both harvesting module variations (to scale, epoxy not shown).

the geometry of the OMHP tubes were machined into the mating surfaces of the heating/cooling blocks to increase contact area. To further decrease thermal contact resistance, the grooves were coated with a thin layer of thermal paste (Omegatherm 201) before the blocks were fastened over the OMHP. Finally, the test assembly was enveloped in fiberglass insulation to reduce heat loss to the environment. In quantifying the thermal performance of the OMHP, it was assumed that all the energy released by the cartridge heaters was transmitted along the OMHP to the water blocks. However, heat loss from the OMHP assembly existed and was found to increase with power input, predominantly near the evaporator. Based on the surface temperature of the insulation, heat loss over the entire OMHP was estimated to be $\leq$5% at higher power inputs. A schematic of the experimental setup is shown in Fig. 3 below.

Thermal and voltage data were collected with a National Instruments cDAQ-9178 data acquisition (DAQ) system using NI-9213 temperature and NI-9205 voltage modules. For a ±200 mV input range, the DAQ voltage module had an absolute accuracy of 174 μV and sensitivity of 4 μV; of these, the sensitivity is most important as all voltage data were offset before analysis so that $V_{avg} = 0$. LabVIEW SignalExpress 2016 was used to read and preprocess data. All TCs were sampled at 100 Hz, while the voltage across the solenoid was sampled at 500 Hz to prevent aliasing. The solenoid voltage was quantified using either the VOC measured through a passive 40 Hz low-pass filter (LPF) to eliminate high-frequency noise, or the voltage measured across a resistor connecting the solenoid leads with no LPF; these respective circuits are shown in Fig. 4. The load resistor in Fig. 4b allowed power produced by the solenoid to be calculated, and it was varied from 665 ± 0.1 Ω (where $V_r \approx$ VOC) to 10.2 ± 0.1 Ω. The noise floor with and without the passive LPF was ~20 μV and ~2 mV, respectively (compared to typical induced voltages on the order of $10^1$–$10^2$ mV). The increase in noise is due to background signals above ~250 Hz in the absence of the physical LPF. However, all phenomena of interest occurred at much lower frequencies [6,19]. For all cases, a digital 45 Hz LPF (40th order Butterworth) was implemented in LabVIEW to remove the prominent 60 Hz signal originating from the cartridge heaters and other nearby electrical wiring.

Tests began at 10 W heat input to demonstrate the OMHP performance without fluid oscillation. The heat input was then increased to 50 W, which was sufficient to produce fluid oscilla-

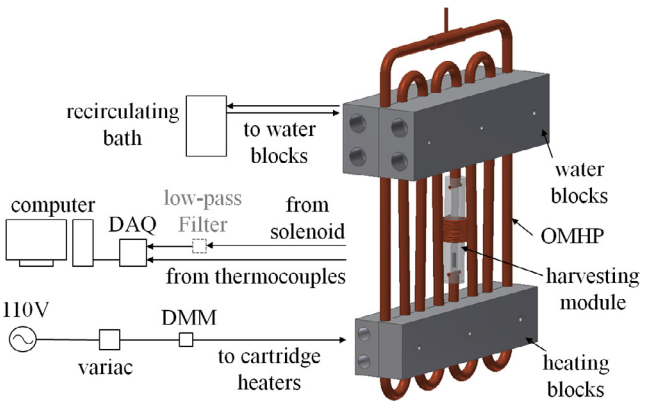


**Fig. 3.** Schematic of OHP experimental setup (fiberglass insulation not shown).

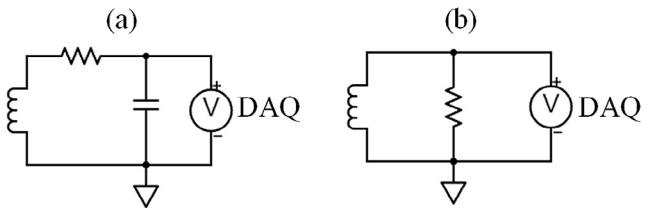


**Fig. 4.** Voltage measurement circuitry for (a) VOC and (b) power.

tion, and continued upwards in 50 W increments until maximum temperature oscillation spikes reached 100 °C. At each power input, the OMHP was allowed to reach quasi-steady state (*i.e.* temperatures oscillating about constant averages) before three minutes of temperature and voltage data were collected. Because HPLC-grade water was used as the working fluid, the pressure inside the OMHP can be estimated based on the saturation pressure of water (*e.g.* at room temperature the pressure inside the OMHP would be approximately $P_{sat}(23\,°C) = 2.8$ kPa). Therefore, the cutoff temperature was set at 100 °C to reduce the chance of seal failure around the harvesting module, since above 100 °C the maximum pressure inside the OMHP would be above 1 atm.

## 3. Results and discussion

### 3.1. Energy harvesting

The energy harvesting ability of the OMHP was quantified using both open-circuit and closed-circuit voltage measurements across the solenoid of the harvester module during OMHP operation (see Fig. 4). Examples of open-circuit voltage responses for the ∅1.59 mm and ∅3.17 mm magnets are shown in Fig. 5 for 200 W heat input. As shown in Fig. 5, not only was $VOC_{\varnothing 3.17mm}$ many times greater (~13×) than $VOC_{\varnothing 1.59mm}$, *i.e.* higher amplitude, but the ∅3.17 mm magnet also oscillated much more consistently.

Fluid oscillations in an OHP occur over a frequency spectrum, but there is a 'dominant' frequency for a given heat input [6]. Therefore, the $OMHP_{3.17}$ voltage is not a typical sinusoidal wave as found from electrical outlets, although the voltage does alternate between positive and negative potentials with quasi-periodicity. Comparatively, the ∅1.59 mm magnet is less synchronized with fluid motion since it only covers ~22% of the channel area; thus, fluid can flow around the magnet without drastically affecting the magnet's momentum (unlike the ∅3.17 mm magnet, which covers ~87% of the flow area). Therefore, the ∅1.59 mm magnet produces voltage pulses that are less regular and smaller than the ∅3.17 mm magnet due to its smaller cross-sectional area and mass (*i.e.* weaker magnetic field), respectively.

To give a more comprehensive representation of the OMHP harvesting ability, the voltage datasets were analyzed three different ways. First, the largest 1% positive and negative voltage data were averaged to estimate $\overline{VOC}_{max}$ and $\overline{VOC}_{min}$, so as to quantify the average peak-to-peak voltage (Eq. (3)). For example, $\overline{VOC}_{pp}$ for $OMHP_{3.17}$ in Fig. 5 is 377 mV, as opposed to $VOC_{pp,max}$ = 522 mV, which overstates the induced voltage.

$$\overline{VOC}_{pp} = \overline{VOC}_{max,1\%} - \overline{VOC}_{min,1\%} \quad (3)$$

Note that when $\overline{VOC}_{pp}$ possesses the same order-of-magnitude as $VOC_{pp,max}$, this indicates more consistent induction. However, in the case of the $OMHP_{1.59}$, $\overline{VOC}_{pp}$ was often drastically different than $VOC_{pp,max}$ due to the erratic magnet behavior. Occasionally, the ∅1.59 mm magnet would produce one or two very large voltage pulses (even as large as the ∅3.17 mm magnet) but would produce small, sporadic pulses for the remainder of the test as seen in Fig. 5. Therefore, Fig. 6 gives both $\overline{VOC}_{pp}$ and $VOC_{pp,max}$ to demonstrate the disparity among voltage pulses. Also included in Fig. 6 is $VOC_{RMS}$, which is used to present the long periods of time between voltage pulses (as seen in Fig. 5). Note that for one of the two tests run at 50 W heat input, a confluence of conditions allowed for a single pulse of nearly $VOC_{pp,max}$ = 90 mV, whereas $\overline{VOC}_{pp}$ for both tests was less than 5 mV.

Due to the irregularity of the ∅1.59 mm magnet oscillation at lower heat inputs, the relation between the closed-circuit $V_s$ and electrical resistance (*i.e.* load) was not measured until 400 W heat input. At this specific heat input, the magnet's motion was more consistent due to increased fluid momentum. The DAQ can be considered an ideal voltmeter (input impedance >10 GΩ), thus the voltage drop across the resistor connecting the solenoid leads (see Fig. 4b) can be used to calculate the power produced in the solenoid using a form of Ohm's law, *i.e.* $P = V^2/R$. Fig. 7 presents the electrical power output vs. electrical resistance based on measurements of $V_{s,pp,max}$ and $V_{s,RMS}$ for the $OMHP_{1.59}$. As with voltages shown in Fig. 6, the average power output in Fig. 7 is much lower than the peak output.

Fig. 8 gives the closed-circuit $\bar{V}_{s,pp}$ and $V_{s,RMS}$ vs. electrical resistance for the $OMHP_{3.17}$. Note that $V_{s,RMS}$ = 9.2 ± 0.5% of $\bar{V}_{s,pp}$ for all test conditions in Fig. 8, whereas $V_{s,RMS}$ = 12.0 ± 3.8% of $\bar{V}_{s,pp}$ for the $OMHP_{1.59}$ in Fig. 6. The relatively constant ratio of $V_{s,RMS}$ to $\bar{V}_{s,pp}$ (varying by less than 0.5%) for $V_{s,RMS,3.17}$ provides further evidence of the ∅3.17 mm magnet's consistent motion, which may be attributed to a low probability of fluid passing through the small flow area between the inner tube and magnet.

The voltage behavior is consistent in both Fig. 8a and b. As heat input increases, so does the voltage across the solenoid. Also, as expected, solenoid voltage decreases with decreasing electrical resistance due to the increase in current. The power output vs. electrical resistance, based on $V_{s,pp,max}$ and $V_{s,RMS}$, is given in Fig. 9. As in Fig. 7, the maximum of the peak and average power outputs both occur at 91 Ω. However, since only a small range of

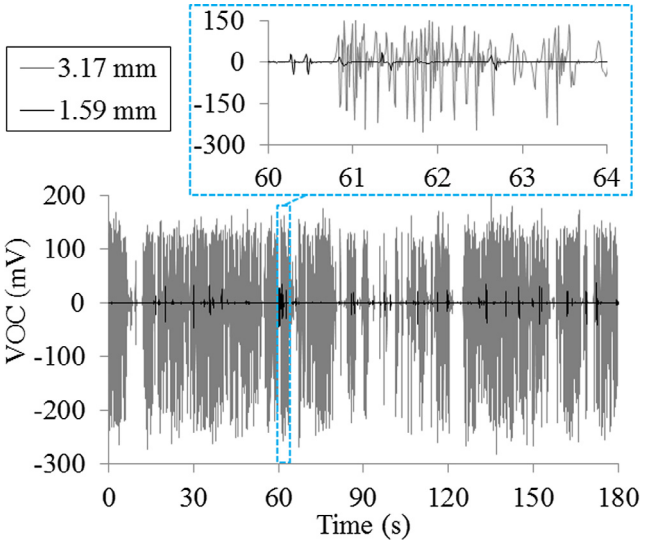


**Fig. 5.** VOC vs. time for $OMHP_{1.59}$ and $OMHP_{3.17}$ at 200 W heat input.

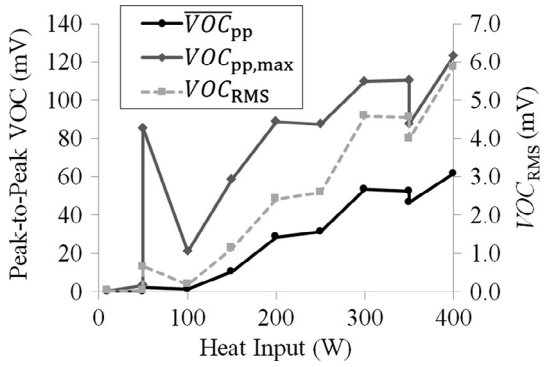


**Fig. 6.** Average and maximum peak-to-peak VOC and $VOC_{RMS}$ vs. heat input for $OMHP_{1.59}$.

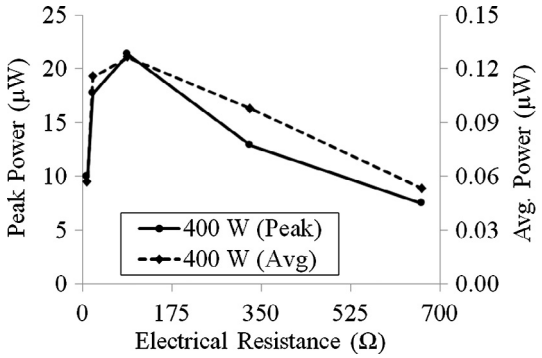


**Fig. 7.** Average and peak electrical power generated vs. electrical resistance for $OMHP_{1.59}$ at 400 W heat input.

electrical resistance was investigated, it cannot be claimed that power output is maximized at 91 Ω. Using the standard means for quantifying efficiency of a heat engine (*i.e.* work delivered per unit heat transfer), and measurements pertaining to the average power output of the $OMHP_{3.17}$ at 200 W heat input, one may determine that the $OMHP_{3.17}$ has a heat engine efficiency of $7.6 \times 10^{-8}$%. Note that the heat transfer through the OMHP is significantly higher than work extracted and, accordingly, it is hard to classify the OMHP as a heat engine; thus, its Carnot efficiency misrepresents its functionality.

### 3.2. Thermal performance

In order to assess the impact of energy harvesting and magnet pressure drop on the OMHP's heat transfer ability, and to characterize the OMHP thermal performance as a whole, an effective, 'per-tube' thermal conductivity, $k_{eff}$, was defined per Eq. (4). This thermal conductivity was calculated using the measured temperature differences across OMHP tubes t3, t5 and t6 based on thermocouple pairs 3 & 5, 6 & 7, and 8 & 10, respectively (all thermocouple locations and tube numbers are shown in Fig. 2). Note that t5 is the tube in which the harvester module is installed. The heat input, $Q$, was assumed to be evenly divided among the eight OMHP tube sections. Note that thermocouples 6 & 7 were applied to bare copper tubing before and after the harvesting module, hence, the same $d_o$ = 4.8 mm was used for all calculations.

$$k_{eff} \approx \frac{Q/8}{\pi/4 d_o^2}\left(\frac{\Delta y}{\Delta T}\right)_i \tag{4}$$

The effective, per-tube thermal conductivity for OMHP tubes t3, t5 and t6, as measured using an open-circuit configuration, is shown in Fig. 10a, while $k_{eff}$ of the harvesting tube during power tests (*i.e.* closed-circuit configuration) is shown in Fig. 10b.

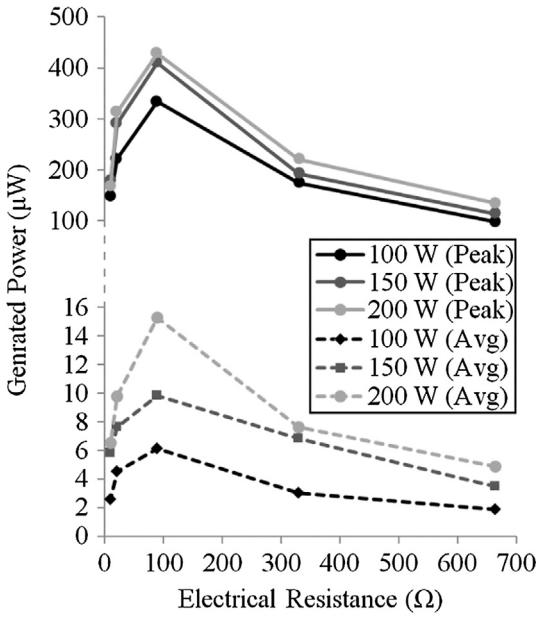


**Fig. 9.** Average and peak electrical power generated vs. electrical resistance for $OMHP_{3.17}$.

It may be seen from Fig. 10a that $k_{eff,t3} \approx k_{eff,t6}$ for both OMHPs and that they are larger than the thermal conductivity of the harvesting tube. Also, the effective thermal conductivity for the OMHP tubes are shown to be on-the-order of 1000–5000 W/m K and to increase with heat input. Based on Fig. 10b, $k_{eff,t5}$ is not a function of the circuit impedance (*i.e.* power production). As shown in Fig. 10a, the OMHP harvesting tube thermal conductivity increases less with heat input than non-harvesting tube sections. The decreased thermal performance of the harvesting tube is most likely due to the increased pressure drop across the harvesting module. This is further evidenced by the poorer thermal performance of the $OMHP_{3.17}$; not only is $k_{eff,\varnothing 3.17mm}$ lower than $k_{eff,\varnothing 1.59mm}$, but the $OMHP_{3.17}$ only managed 200 W of heat input before reaching an external, peak surface temperature of 100 °C. The flow within the $OMHP_{3.17}$ is more similar to a paired 2.5-turn and 1.5-turn open-loop OHP than a 4-turn closed-loop OHP. Hence, the ability for condensate to circulate between adjacent tubes of the OHP is limited and the heat transfer ability should decrease to some degree [31,32]. Based on the similarity between $k_{eff,t3}$ and $k_{eff,t6}$, proximity to the harvesting tube does not appear to

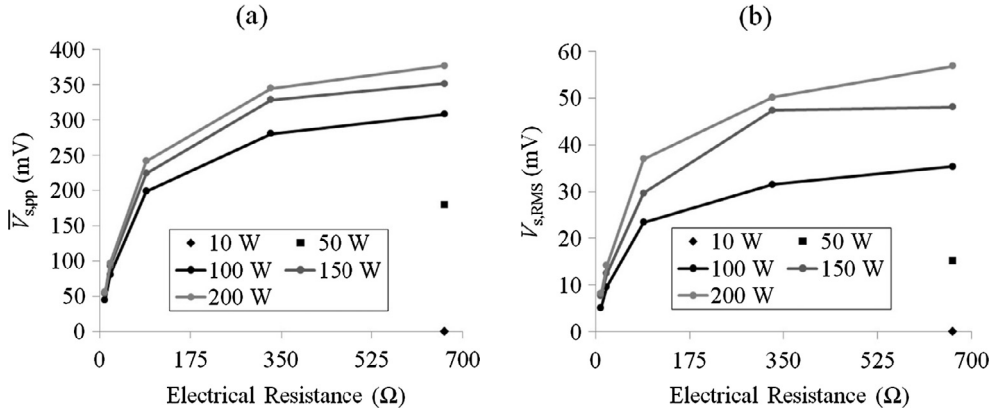


**Fig. 8.** (a) Average peak-to-peak voltage and (b) $V_{s,RMS}$ vs. electrical resistance for $OMHP_{3.17}$.

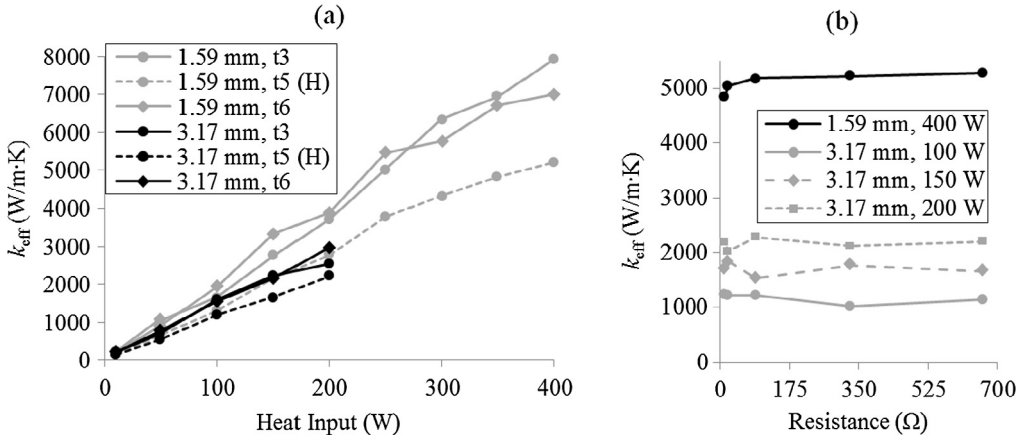


**Fig. 10.** Effective thermal conductivity for (a) three tubes of the $OMHP_{1.59}$ and $OMHP_{3.17}$ vs. heat input for open circuit configuration and (b) the harvesting (H) tube (t5) of the $OMHP_{1.59}$ and $OMHP_{3.17}$ vs. electrical resistance during closed circuit configuration.

affect the per-tube thermal performance. The observed variation in $k_{eff}$ between the harvesting and non-harvesting tubes should not be wholly attributed to the decreased thermal conductivity of the polycarbonate tube section, as wall conduction has been shown to contribute less than 10% of the overall heat transferred in a tubular OHP of similar design [6].

The pressure drop in the annular flow along the length of the harvesting magnets (6.35 mm) was estimated analytically using the hydraulic diameter $d_h = d_i - d_{mag}$ (where $d_i$ = 3.4 mm in the polycarbonate tube section). The entrance and exit effects of the annular flow were not considered. The equation for major pressure loss along a pipe was used, *i.e.*:

$$\Delta P = L \cdot f_d \cdot \frac{\rho}{2} \cdot \frac{V^2}{d_h} \tag{5}$$

where $f_d$ is the Darcy friction factor. For $Re_D < 2000$ (laminar flow), $f_d = 64/Re_D$; while the Haaland equation [33] was used to calculate $f_d$ for $Re_D > 4000$ (turbulent flow). During transitional flow, *i.e.* $2000 < Re_D < 4000$, an average was computed using the laminar and turbulent $f_d$ (denoted by dashed lines in Fig. 11a). Water properties were evaluated assuming saturation conditions at 62 °C; which is a representative temperature of the $OMHP_{1.59}$ and $OMHP_{3.17}$ harvesting modules at ~200 W. Fig. 11a shows the pressure drop calculated using Eq. (5) for the two magnets and a section of open polycarbonate tubing of equal length. The pressure drop is plotted in Fig. 11a until all three flows transition to turbulence. Because the flow velocity and $d_h$ varies for the two magnets and the bare polycarbonate tube, flow rate is provided on the primary *x*-axis in Fig. 11, with the corresponding fluid velocity (in the bare copper tube on either side of the harvester module) given on the secondary *x*-axis. To provide easier comparison among the curves in Fig. 11a, their ratios are shown in Fig. 11b.

It can be seen in Fig. 11b that the pressure drop around the ∅3.17 mm magnet is at least two orders-of-magnitude greater than that around the ∅1.59 mm magnet (average of ~320×), which in turn is only 2.5–4.5 times greater than an open tube. Note that the pressure drops in Fig. 11 do not include the losses caused by the transverse posts, which each cover ~62% of the area within the copper tubes joining the harvesting module. These results demonstrate the hydrodynamic coupling of the OHP energy harvester. Higher pressure drops across the employed magnet implies that pressure 'shorting' (*i.e.* flow between magnet and tube internal surface) is less likely and that linear momentum transfer between the pulsating fluid and magnet is more achievable. A hydrodynamic and/or smaller magnet would reduce such momentum transfer, but would allow for better heat transfer within that region since more flow would exist along the tube internal surface.

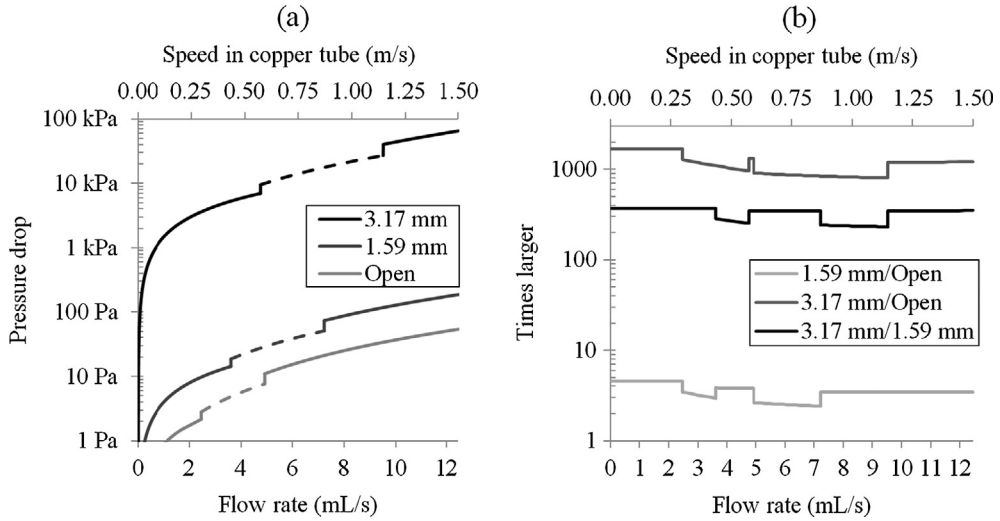


**Fig. 11.** (a) Estimated pressure drop along annulus surrounding induction magnets for saturated liquid water at 62 °C vs. flow rate compared with pressure drop for same length of open polycarbonate tube; transitional flow denoted by dashed lines (b) ratio of pressure drops.

## 4. Conclusions

A 4-turn 'oscillating-magnet' OHP (OMHP) was designed and tested for thermal-to-electric energy harvesting. Either a ∅1.59 mm or ∅3.17 mm, 6.35 mm long NdFeB-N52 magnet in-line with the OMHP fluid flow was used for electromagnetic induction in a 1000-turn, coaxial solenoid wrapped around a single section of an OHP tube. Several relationships among OMHP heat input, induction magnet size, thermal performance, induced VOC, and electrical power output were determined. These findings are summarized below.

1. Over a heat input range of 10–200 W, the effective thermal conductivity of the $OMHP_{1.59}$ was approximately 30% higher than that of the $OMHP_{3.17}$. Moreover, the $OMHP_{3.17}$ reached an external surface temperature of 100 °C at 200 W heat input, while the $OMHP_{1.59}$ achieved such a temperature at 400 W of heat input. This is likely due to the pressure drop across the ∅3.17 mm magnet being >2 orders-of-magnitude higher than that across the ∅1.59 mm magnet.
2. The effective thermal conductivity of non-harvesting tubes was on average 42% and 35% higher than the harvesting tube for the $OMHP_{1.59}$ and $OMHP_{3.17}$, respectively.
3. Varying the electrical resistance across the solenoid leads had no discernible effect on effective thermal conductivity of the OMHP harvesting tube.
4. The motion of the ∅1.59 mm magnet (and therefore its induced voltage) was more inconsistent than the ∅3.17 mm magnet. Since the ∅3.17 mm magnet covered 87.2% of the flow area in the harvesting module, as compared to 21.8% for the ∅1.59 mm magnet, the motion of the ∅3.17 mm magnet was more closely coupled with the fluid motion.
5. Due to the sporadic motion of the ∅1.59 mm magnet, it only produced a peak and average power output of 21 μW and 0.126 μW, respectively, within the harvesting module of the OMHP. This occurred at 400 W of heat input, whereas the $OMHP_{3.17}$ produced a peak and average power output of 428 μW and 15.3 μW, respectively, at 200 W of heat input.
6. For both OMHPs, the measured output voltage decreased with solenoid/DAQ electrical resistance.

Unlike traditional thermoelectric devices, the OMHPs presented in this work maintained very high heat transfer capability while producing electric power. The $OMHP_{3.17}$ thermally underperformed the $OMHP_{1.59}$, yet still achieved a maximum, effective thermal conductivity of ~2600 W/m K. Although the reported OMHP power generation rate is small (~0.1 mW) relative to dedicated energy harvesting technologies, the inspected OMHP is a non-optimized, proof-of-concept prototype. Due to the OMHP being a new heat transfer platform, there is a lot to be learned in terms of the applications where it can have the most impact. One possible application is the recharging of a sensor or communication device capacitor via a given temperature difference (or waste heat input). This can be especially important in remote areas where power grids are unavailable. Another example is its integration into microelectromechanical systems and small scale robotics where thermal management and in-situ power supply are needed.

## Acknowledgements

This work was sponsored in part by the National Science Foundation under Awards CBET-1403872, ECCS-1549973 and ECCS-1660446. ERDC did not fund or endorse the research disclosed herein.

## References

[1] H. Akachi, Structure of a heat pipe, 4921041, 1990.
[2] H.B. Ma, C. Wilson, B. Borgmeyer, K. Park, Q. Yu, S.U.S. Choi, M. Tirumala, Effect of nanofluid on the heat transport capability in an oscillating heat pipe, Appl. Phys. Lett. 88 (2006) 1–3, https://doi.org/10.1063/1.2192971.
[3] O. Suzuki, Heat-transport characteristics of a bubble-driven non-looped heat-transport device, Trans. Japan Soc. Mech. Eng. Part B 69 (2003) 430–436, https://doi.org/10.1248/cpb.37.3229.
[4] H.B. Ma, B. Borgmeyer, P. Cheng, Y. Zhang, Heat transport capability in an oscillating heat pipe, J. Heat Transfer. 130 (2008) 1–7, https://doi.org/10.1115/1.2909081.
[5] J.D. Fairley, S.M. Thompson, D. Anderson, Time–frequency analysis of flat-plate oscillating heat pipes, Int. J. Therm. Sci. 91 (2015) 113–124, https://doi.org/10.1016/j.ijthermalsci.2015.01.001.
[6] J.G. Monroe, Z.S. Aspin, J.D. Fairley, S.M. Thompson, Analysis and comparison of internal and external temperature measurements of a tubular oscillating heat pipe, Exp. Therm. Fluid Sci. 84C (2017) 165–178, https://doi.org/10.1016/j.expthermflusci.2017.01.020.
[7] J.L. Xu, X.M. Zhang, Start-up and steady thermal oscillation of a pulsating heat pipe, Heat Mass Transf. Und Stoffuebertragung. 41 (2005) 685–694, https://doi.org/10.1007/s00231-004-0535-3.
[8] W. Qu, H. Ma, Theoretical analysis of startup of a pulsating heat pipe, Int. J. Heat Mass Transf. 50 (2007) 2309–2316, https://doi.org/10.1016/j.ijheatmasstransfer.2006.10.043.
[9] M. Groll, S. Khandekar, Pulsating heat pipes: a challenge and still unsolved problem in heat pipe science, Arch. Thermodyn. 23 (2002) 17–28. http://baztech.icm.edu.pl/baztech/cgi-bin/btgetdoc.cgi?BGPK-0379-2630.
[10] H. Ma, Oscillating Heat Pipes, first ed., Springer-Verlag New York, New York, 2015, doi:10.1007/978-1-4939-2504-9.
[11] H. Yang, S. Khandekar, M. Groll, Operational limit of closed loop pulsating heat pipes, Appl. Therm. Eng. 28 (2008) 49–59, https://doi.org/10.1016/j.applthermaleng.2007.01.033.
[12] H.B. Ma, C. Wilson, Q. Yu, K. Park, U.S. Choi, M. Tirumala, An Experimental investigation of heat transport capability in a nanofluid oscillating heat pipe, J. Heat Transfer 128 (2006) 1213, https://doi.org/10.1115/1.2352789.
[13] M. Furukawa, Rationalized concise descriptions of fluid motions in an oscillating/pulsating heat pipe, J. Heat Transfer 136 (2014), https://doi.org/10.1115/1.4027553.
[14] G. Mahajan, S.M. Thompson, H. Cho, Energy and cost savings potential of oscillating heat pipes for waste heat recovery ventilation, Energy Rep. 3 (2017) 46–53, https://doi.org/10.1016/j.egyr.2016.12.002.
[15] Q. Wang, Z. Rao, Y. Huo, S. Wang, Thermal performance of phase change material/oscillating heat pipe-based battery thermal management system, Int. J. Therm. Sci. 102 (2016) 9–16, https://doi.org/10.1016/j.ijthermalsci.2015.11.005.
[16] X. Han, H. Ma, A. Jiao, J.K. Critser, Investigations on the heat transport capability of a cryogenic oscillating heat pipe and its application in achieving ultra-fast cooling rates for cell vitrification cryopreservation, Cryobiology 56 (2008) 195–203, https://doi.org/10.1016/j.cryobiol.2008.02.006.
[17] S.M. Thompson, B.S. Tessler, H. Ma, D.E. Smith, A. Sobel, Ultrahigh thermal conductivity of three-dimensional flat-plate oscillating heat pipes for electromagnetic launcher cooling, IEEE Trans. Plasma Sci. 41 (2013) 1326–1331, https://doi.org/10.1109/TPS.2013.2244920.
[18] D. Zabek, J. Taylor, V. Ayel, Y. Bertin, C. Romestant, C.R. Bowen, A novel pyroelectric generator utilising naturally driven temperature fluctuations from oscillating heat pipes for waste heat recovery and thermal energy harvesting, J. Appl. Phys. 120 (2016), https://doi.org/10.1063/1.4958338.
[19] J.G. Monroe, E.S. Vasquez, Z.S. Aspin, K.B. Walters, M.J. Berg, S.M. Thompson, Electromagnetic induction by ferrofluid in an oscillating heat pipe, Appl. Phys. Lett. 106 (2015) 263901, https://doi.org/10.1063/1.4923400.
[20] C. Chen, S. Wang, C. Wu, C. Lin, K. Huang, Characteristics of electromagnetic induction by moving ferrofluids, Magnetohydrodynamics 48 (2012) 567–580.
[21] A. Bibo, R. Masana, A. King, G. Li, M.F. Daqaq, Electromagnetic ferrofluid-based energy harvester, Phys. Lett. Sect. A Gen. At. Solid State Phys. 376 (2012) 2163–2166, https://doi.org/10.1016/j.physleta.2012.05.033.
[22] C.L. Sansom, P. Jones, R.A. Dorey, C. Beck, A. Stanhope-Bosumpim, J. Peterson, Synthesis and characterization of Mn0.5Zn0.5Fe 2O4 and Fe3O4 nanoparticle ferrofluids for thermo-electric conversion, J. Magn. Magn. Mater. 335 (2013) 159–162, https://doi.org/10.1016/j.jmmm.2013.02.012.
[23] J. Wang, W. Wang, G.W. Jewel, Design and experimental characterisation of a linear reciprocating generator, IEE Proc. - Electr. Power Appl. 145 (1998) 509–518.
[24] S.R. Vetorino, J.V. Platt, D.A. Springer, Renewable energy flashlight, US 6220719 B1, 2001.
[25] H. Polinder, M.E.C. Damen, F. Gardner, Linear PM generator system for wave energy conversion in the AWS, IEEE Trans. Energy Convers. 19 (2004) 583–589, https://doi.org/10.1109/TEC.2004.827717.
[26] K. Rhinefrank, E.B. Agamloh, A. Von Jouanne, A.K. Wallace, J. Prudell, K. Kimble, J. Aills, E. Schmidt, P. Chan, B. Sweeny, A. Schacher, Novel ocean energy permanent magnet linear generator buoy, Renew. Energy 31 (2006) 1279–1298, https://doi.org/10.1016/j.renene.2005.07.005.
[27] X. Jiang, Y. Li, J. Li, Design of a novel linear permanent magnet vibration energy harvester, in: 2013 IEEE/ASME Int. Conf. Adv. Intell. Mechatronics, 2013, pp. 1090–1095, doi:10.1109/AIM.2013.6584239.

[28] J.A. Konotchick, Linear Motion Electric Power Generator, US5347186 A, 1994.
[29] Z. Xu, S. Chang, Prototype testing and analysis of a novel internal combustion linear generator integrated power system, Appl. Energy 87 (2010) 1342–1348, https://doi.org/10.1016/j.apenergy.2009.08.027.
[30] S. Khandekar, N. Dollinger, M. Groll, Understanding operational regimes of closed loop pulsating heat pipes: An experimental study, Appl. Therm. Eng. 23 (2003) 707–719, https://doi.org/10.1016/S1359-4311(02)00237-5.
[31] H. Yang, S. Khandekar, M. Groll, Performance comparison of open loop and closed loop pulsating heat pipes, in: Proceedings of the 8th International Heat Pipe Symposium, Kumamoto, Japan, September 24–27.
[32] C. Wilson, B. Borgmeyer, R.A. Winholtz, H.B. Ma, D. Jacobson, D. Hussey, Thermal and visual observation of water and acetone oscillating heat pipes, J. Heat Transfer 133 (2011) 61502, https://doi.org/10.1115/1.4003546.
[33] S.E. Haaland, Simple and explicit formulas for the friction factor in turbulent pipe flow, J. Fluids Eng. 105 (1983) 89, https://doi.org/10.1115/1.3240948.